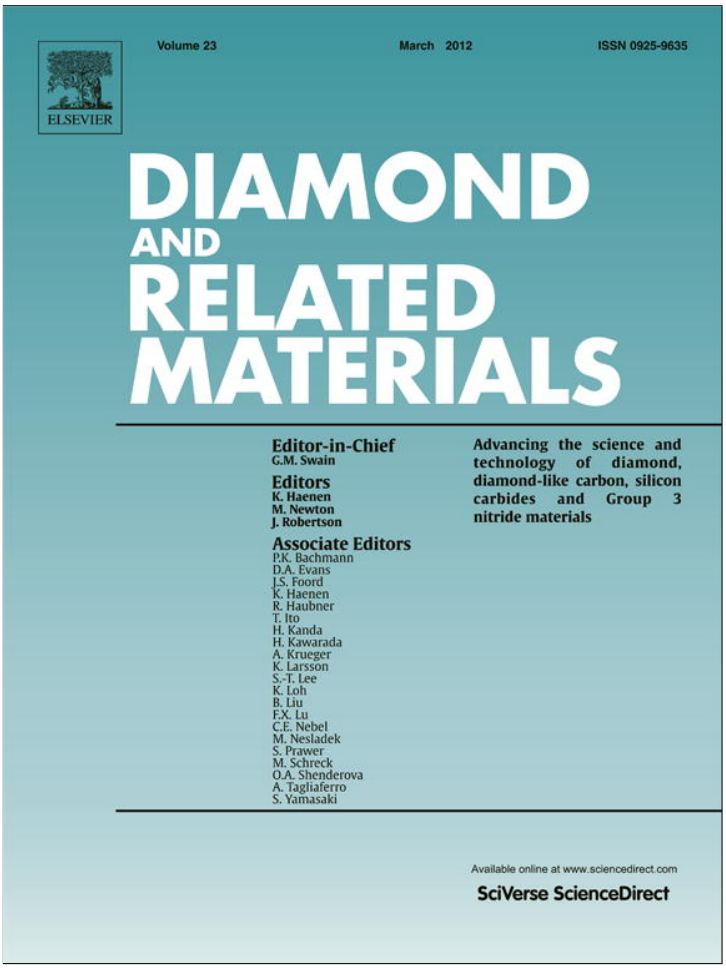

Diamond & Related Materials 23 (2012) 150–153

Contents lists available at SciVerse ScienceDirect

Diamond & Related Materials

journal homepage: www.elsevier.com/locate/diamond

# Magnetic resonance study of nanodiamonds prepared by laser-assisted technique ☆

A.M. Panich [a,*], A.I. Shames [a], B. Zousman [b], O. Levinson [b]

[a] Department of Physics, Ben-Gurion University of the Negev, P.O. Box 653, Be'er Sheva 84105, Israel
[b] Ray Techniques Ltd., High Tech Village, The Hebrew University, P.O.B. 39162, Jerusalem 91391, Israel

ARTICLE INFO

Available online 6 January 2012

*Keywords:*
Nanodiamond
NMR
EPR
Laser-assisted technique

ABSTRACT

We present XRD, $^{1}$H and $^{13}$C NMR and EPR characterization of nanodiamond samples fabricated using laser treatment of carbon soot. We show that the samples are of high quality and nearly metal- and graphite-free. Variations in the EPR spectra and $^{13}$C nuclear spin–lattice relaxation times with increased grain size are obtained.



## 1. Introduction

Diamond nanoparticles have great potential for a variety of materials applications [1–3]. They are currently produced in bulk quantities by means of detonation of carbon-containing explosives followed by purification of the detonation soot by chemical treatment.

Another way of the nanodiamond (ND) production utilizes a laser irradiation of water suspension of graphite powders at room temperature and normal pressure, which yields the ND particles of 3–6 nm in size [4]. However, such a technique is less widespread compared with the detonation one, and the samples obtained are less studied compared with the detonation NDs. In this paper, we present XRD, NMR and EPR characterization of the ND samples of different size, varying from 5 to 100–300 nm, fabricated from carbon soot by using a laser-assisted technique. The samples are non-toxic, reveal unique photoluminescence, high adsorption potential and ability to interact with biomolecules. We show that our samples are of high quality and nearly metal- and graphite-free. Variations in the EPR spectra and $^{13}$C nuclear spin–lattice relaxation times with increased grain size are obtained.

## 2. Experimental details

Two samples with the grain size of 5.3 nm (ND1) and of 100–300 nm (ND2) were fabricated from carbon soot using a laser-assisted technique developed by Ray Techniques Ltd. The method is based on a high-intensive laser irradiation of a target containing non-diamond carbon soot placed in a liquid media. Nd:YAG pulse laser with a wavelength of 1064 nm and laser pulses with the length of several nanoseconds were used. Short laser pulses of high intensity affect a soot-containing target and cause high local gradients of temperature and pressure. This results in formation of mono-dispersed ND particles. Variation of the power of laser radiation causes variation of the ND dimension. The larger particles are prepared at larger density of the luminous flux of laser. Then NDs were isolated and cleaned by flotation in de-ionized water, washed and dried. This technique results in synthesis of the metal-free NDs. For comparison, we also measured a sample of detonation nanodiamond (DND) with the grain size of ~5 nm.

All NMR and EPR data have been collected at room temperature. The $^{13}$C MAS (magic angle spinning) HPDEC (high power decoupling) NMR measurements with spinning sideband suppression have been carried out at a resonance frequency of 125.8 MHz ($B_0 = 11.744$ T) with a spinning rate of 12 kHz. Static $^{1}$H spectra, $^{1}$H and $^{13}$C spin–lattice ($T_1$) and spin–spin ($T_2$) relaxation times have been measured in an applied magnetic field $B_0 = 8.0196$ T at resonance frequencies of 341.41 MHz for $^{1}$H and 85.85 MHz for $^{13}$C respectively. $^{13}$C chemical shifts are referenced to tetramethylsilane (TMS).

## 3. Results and discussion

X-ray diffraction patterns of NDs (Fig. 1) reveal diffraction maxima at the angles $2\theta = 43.9$ and 75.4 corresponding to (111) and (220) reflections of a diamond lattice with $a_0 = 3.565$ Å. The observed peak broadening for ND1 sample in comparison with ND2 is characteristic for small nano-particles. The average size of diamond crystallites under study, estimated using the Scherrer formula, was found to be 5.3 nm for ND1 and 115 nm for ND2 samples, respectively. HRTEM image of ND2 particles shows the grain size from 100 to 300 nm.

Room temperature EPR spectra are shown in Fig. 2. The sample ND1 reveals a Lorentzian-like singlet ascribed to the unpaired electron spins of dangling bonds. DND sample shows very similar EPR spectrum. The EPR signal of the ND2 sample is a superposition of two components of the nearly same intensities. The first, a singlet Lorentzian, originates

☆ Presented at the Diamond 2011, 22nd European Conference on Diamond, Diamond-Like Materials, Carbon Nanotubes, and Nitrides, Budapest.

* Corresponding author.
*E-mail address:* pan@bgu.ac.il (A.M. Panich).

0925-9635/$ – see front matter © 2012 Elsevier B.V. All rights reserved.
doi:10.1016/j.diamond.2011.12.047

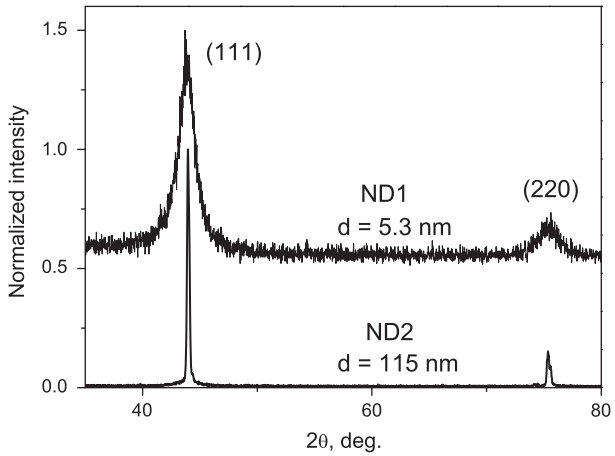


**Fig. 1.** XRD patterns of ND1 and ND2 samples.

from the unpaired electron spins of the dangling bonds. The second, a well resolved polycrystalline hyperfine pattern, originates from so-called P1 or $N^0$ paramagnetic center arising from a single unpaired electron interacting with the $^{14}N$ nuclear spin ($I=1$). Integral intensities of both components in the ND2 sample are practically the same. EPR measurements reveal $N_S=(7.3\pm0.8)\times10^{19}$ spin/g for the samples ND1 and DND and $N_S=(2.4\pm0.3)\times10^{19}$ for the sample ND2, that correspond to ~15 spins per small ND1 particle and more than $3\times10^5$ spins per large ND2 particle of the average size of 200 nm. It was found that the total amount of spins in ND1 insignificantly (within 5%) depends on degassing and in both ND1 and ND2 it is practically independent on such samples' processing as acid cleaning. It means that the vast majority of uncoupled electron spins are located in the diamond bulk rather than on the surface.

**Table 1**
$^{13}C$ spin–lattice and spin–spin relaxation times in ND samples.

| Sample | $T_1$, s | α | $T_{2core}$, ms | $T_{2shell}$, ms |
|---|---|---|---|---|
| ND1 | 0.35 ± 0.02 | 0.65 ± 0.02 | 1.67 ± 0.05 | 0.206 ± 0.017 |
| ND2 | 30.8 ± 2 | 0.61 ± 0.01 | 2.79 ± 0.26 | 0.60 ± 0.02 |

$^{13}C$ MAS spectra of three ND samples are shown in Fig. 3. ND2 sample reveals very narrow line (line width $\Delta\nu$~1 ppm) at 35.1 ppm characteristic of $sp^3$ carbons of bulk diamond. The spectra of ND1 and DND are very similar. Both ND1 and DND samples reveal an intense peak at 34.4 ppm, which is definitely assigned to the $sp^3$ carbon atoms of the diamond core. In the ND1 sample, a very weak additional peak (marked by an arrow) appears at the $sp^2$ carbon position, $\sigma=130$ ppm. These aromatic carbons account for 0.5% of all carbon

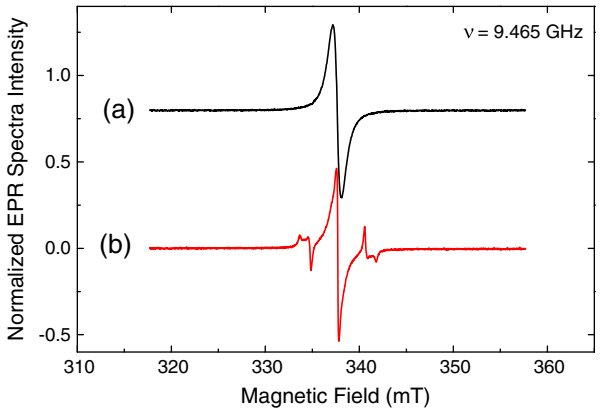


**Fig. 2.** EPR spectra of (a) ND1 and (b) ND2 samples.

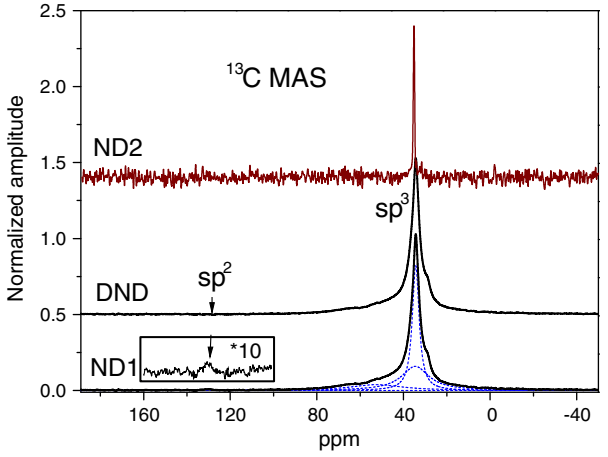


**Fig. 3.** $^{13}C$ MAS HPDEC NMR spectra of ND1, DND and ND2 samples with spinning sideband suppression. Deconvolution of the ND1 spectrum in four components is shown by dashed lines. Peak at the $sp^2$ carbon position is marked by an arrow. Magnified signal of $sp^2$ carbon atoms is shown in Inset.

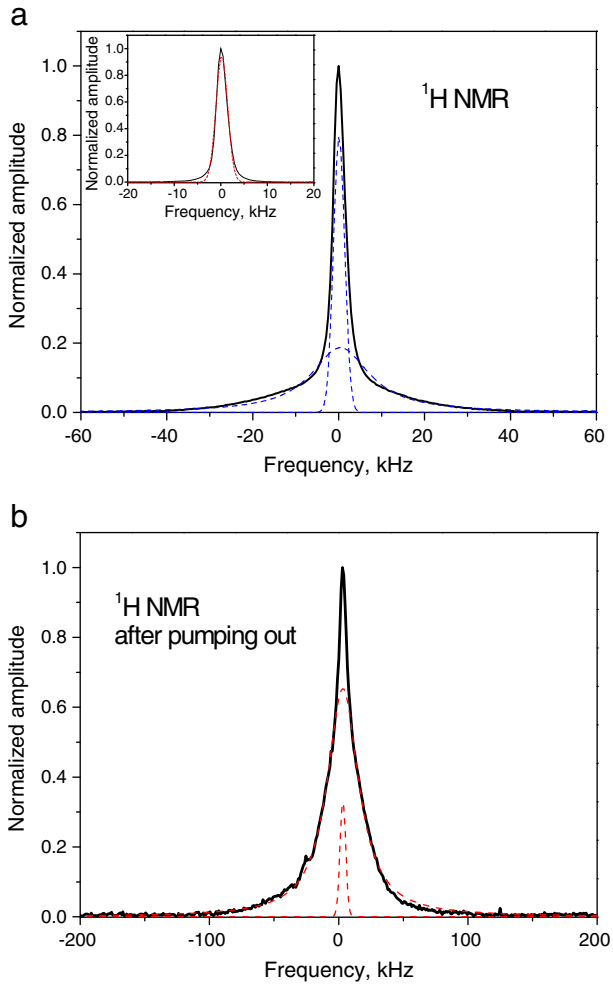


**Fig. 4.** Static $^1H$ NMR spectra of ND1 sample (a) before and (b) after pumping out down to $10^{-5}$ Torr at room temperature. Deconvolution into two components is shown by dashed lines. The separately detected narrow component is shown in inset.

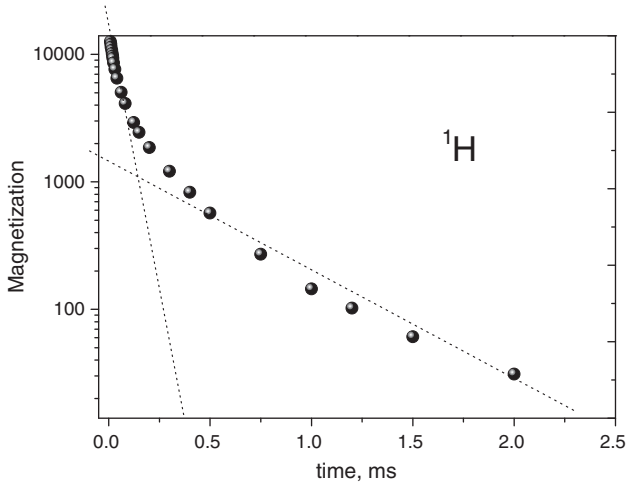


**Fig. 5.** $^1$H spin echo decay ($T_2$ measurements) of the ND1 sample on semi-logarithmic scale.

atoms in the sample. In ND1 and DND, the intense peak at $\delta = 34.4$ ppm is asymmetric and could, in principle, be deconvoluted into three components shown by dashed lines. The narrow line having a chemical shift of $\delta = 34.4$ ppm and a line width of $\Delta\nu = 3.8$ ppm, which is characteristic of bulk diamond, is definitely attributed to the $sp^3$-carbons of the diamond core. (Here and later on the line widths were determined from a Lorentzian fit). The broader line with the similar chemical shift, $\delta = 34.6$ ppm and line width $\Delta\nu = 15.3$ ppm is attributed to somewhat nonequivalent carbon atoms of the diamond core; this inequivalency may result from some distortion of the tetrahedral $sp^3$ coordination. The broad line showing $\delta = 52.5$ ppm and line width $\Delta\nu = 29.2$ ppm probably originates from a disordered carbon shell that covers the diamond core. We note that the ND2 sample reveals very narrow line without this tail, meaning that the larger the particle the more perfect it is and the smaller the relative weight of the shell.

$^{13}$C nuclear spin–lattice relaxation measurements of all samples show that the magnetization recovery is well described by a stretched exponential

$$M(t) = M_\infty \left\{ 1 - \exp\left[ -\left( \frac{t}{T_1} \right)^{\alpha} \right] \right\}, \quad (1)$$

where $M_\infty$ is the equilibrium magnetization. At that, measurements yield different relaxation times for smaller and larger NDs. While the small ND1 sample of the size of 5 nm reveals $T_1 = 349 \pm 16$ ms and $\alpha = 0.65 \pm 0.02$ that is usually observed in the DNDs of such size, the larger ND2 of the size of 100–300 nm reveals $T_1 = 30.8 \pm 2$ s ($\alpha = 0.61 \pm 0.01$) (Table 1). At that, both $T_1$'s are much shorter than those of bulk natural diamond, which vary from several hours to days [5–8]. This significant reduction in the $^{13}$C spin–lattice relaxation time and the stretched exponential character of the magnetization recovery is attributed to the interaction of nuclear spins with paramagnetic defects detected by EPR. Elongation of the spin–lattice relaxation time with increase in particle size seems to be a characteristic property of NDs. While $T_1$ for small DNDs of 4–5 nm in size varies in the range of 270 to 610 ms [9–15], larger NDs measured in this work reveal two orders of magnitude longer $T_1$. This conclusion is supported by our recent data [16] showing that as the size of the diamond particles increases from 4–5 to 10–30 and then to 100–300 nm, nuclear relaxation times become longer, and by the data of Alam [17], who found that NDs of the size of 100–450 nm exhibit $T_1$ of 12 to 45 s. $^{13}$C spin–spin relaxation times $T_2$, attributed to the diamond core and to the shell are given in Table 1.

Occurrence of hydrogen atoms at the ND surface is well seen in the $^1$H NMR measurements. Static $^1$H NMR spectrum of the as-prepared ND samples consists of two lines (Fig. 4a). The broad component with the line width $\Delta\nu = 16.5$ kHz for the sample ND1 and 17.6 kHz for ND2 is attributed to closely set rigid hydrocarbon and hydroxyl groups, while the narrow component showing $\Delta\nu = 2.6$ and 3.0 kHz for the samples ND1 and ND2, respectively, is mainly assigned to the moisture adsorbed on the DND surface and, perhaps, partially to some isolated C–H and C–OH groups. The obtained broad symmetric line reflects strong dipole–dipole interactions among the $^1$H spins that indicate clustering of the hydrogen atoms. Thus one can suggest that the hydrogenated spots of limited sizes alternate with nearly non-hydrogenated zones on the ND surface. Similar clustering of hydrogen and fluorine atoms has recently been observed in initial DND [12,18] and in fluorinated DND [13], respectively. We note that interaction of nuclei with unpaired electrons would yield very broad and highly asymmetric line, which is not observed in our experiment.

The assignment of the narrow component is based on two facts [18]: first, the DND surface is known to be hydrophilic; second, pumping out the sample at room temperature down to $10^{-5}$ Torr effectively reduces the intensity of the narrow component (Fig. 4b) reflecting significant reduction of the moisture content. One can definitely distinguish between narrow and broad lines by measuring the $^1$H NMR spectra with dipolar dephasing, using a long delay between the pulses of spin echo that significantly exceeds the spin–spin relaxation time $T_2$ of the broad line. This makes the broad component to disappear and allows detection of the narrow component only (inset in Fig. 4a).

$^1$H spin–spin relaxation time ($T_2$) measurements show that the magnetization decay in the samples under study is well described by a superposition of two exponentials corresponding to the two resonance lines observed in the experiment and attributed to the two kinds of hydrogen species. It is clearly seen from the semi-logarithmic plot of the magnetization decay (Fig. 5). Here, the longer $T_{21}$ is assigned to the narrower NMR line, while the shorter $T_{22}$ is assigned to the broader line (Table 2).

## 4. Summary

We have carried out XRD, $^1$H and $^{13}$C NMR and EPR investigation of diamond nanoparticles prepared by laser-assisted technique. Experiments with as-prepared and pumped out samples allow distinguishing between moisture and other hydrogen-containing groups. Significant reduction in the $^{13}$C spin–lattice relaxation time compared with natural diamond and stretched exponential behavior of the $^{13}$C magnetization recovery found in the spin–lattice relaxation measurements are attributed to the interaction of nuclear spins with the paramagnetic defects. The magnetic resonance parameters of the small NDs prepared by the laser-assisted technique are very similar to those of DND. Noticeable change of the EPR spectrum and elongation

**Table 2**
$^1$H spin–lattice and spin–spin relaxation times for narrow and broad resonances of ND samples.

| Sample | $T_{1nar}$, s | $T_{1br}$, s | α | $T_{2nar}$, ms | $T_{2br}$, ms | $\Delta\nu_{nar}$, kHz | $\Delta\nu_{br}$, kHz |
|---|---|---|---|---|---|---|---|
| ND1 | 2.66 ± 0.1 | 7.57 ± 0.42 | 0.62 ± 0.02 | 0.40 ± 0.03 | 0.048 ± 0.002 | 2.62 | 16.5 |
| ND2 | 9.7 ± 0.5 | 5.3 ± 0.2 | 0.72 ± 0.03 | 0.68 ± 0.06 | 0.058 ± 0.005 | 3.93 | 23.3 |
| ND2 pumped out | 17.1 ± 2.5 | 5.2 ± 1.56 | 0.85 ± 0.15 | 0.37 ± 0.05 | 0.038 ± 0.002 | 3.94 | 23.3 |

of the $1^3$C spin–lattice relaxation time with increased ND size are obtained.

## Acknowledgments

The work in Ben-Gurion University was partially supported by the New Energy Development Organization of Japan (NEDO) grant #04IT4 and MOST-RFBR grant #3-5708. We thank Roy Hoffman for recording the $^{13}$C MAS spectra and D. Mogilyansky for discussion on the X-ray data.

## References

[1] O. Shenderova, D. Gruen (Eds.), Ultrananocrystalline Diamond: Synthesis, Properties and Applications, William-Andrew, Norwich, NY, 2006, p. 600.
[2] O.A. Shenderova, V.V. Zhirnov, D.W. Brenner, Cr. Rev. Solid State Mater. Sci. 27 (2002) 227–356.
[3] A. Krueger, Chemistry 14 (2008) 1382–1390.
[4] J. Sun, S.-L. Hu, X.-W. Du, Y.-W. Lei, L. Jiang, Appl. Phys. Lett. 89 (2006) 183115/1-3.
[5] M.J.R. Hoch, E.C. Reynhardt, Phys. Rev. B 37 (1988) 9222–9226.
[6] E.C. Reynhardt, C.J. Terblanche, Chem. Phys. Lett. 269 (1997) 464–468.
[7] C.J. Terblanche, E.C. Reynhardt, J.A. van Wyk, Chem. Phys. Lett. 310 (1999) 97–102.
[8] P.M. Henrichs, M.L. Cofield, R.H. Young, J.M. Hewitt, J. Magn. Reson. 58 (1984) 85–94.
[9] A.I. Shames, A.M. Panich, W. Kempiński, A.E. Alexenskii, M.V. Baidakova, A.T. Dideikin, V.Yu. Osipov, V.I. Siklitski, E. Osawa, M. Ozawa, A.Ya. Vul', J. Phys. Chem. Solids 63 (2002) 1993–2001.
[10] A.M. Panich, A.I. Shames, H.-M. Vieth, E. Ōsawa, M. Takahashi, A.Ya. Vul', Eur. Phys. J. B 52 (2006) 397–402.
[11] G. Cunningham, A.M. Panich, A.I. Shames, I. Petrov, O. Shenderova, Diamond Relat. Mater. 17 (2008) 650–654.
[12] A.M. Panich, Diamond Relat. Mater. 16 (2007) 2044–2049.
[13] A.M. Panich, H.-M. Vieth, A.I. Shames, N. Froumin, E. Ōsawa, A. Yao, J. Phys. Chem. C 114 (2010) 774–782.
[14] M. Dubois, K. Guerin, E. Petit, N. Batisse, A. Hamwi, N. Komatsu, J. Giraudet, P. Pirotte, F. Masin, J. Phys. Chem. C 113 (2009) 10371–10378.
[15] A.M. Panich, A.I. Shames, O. Medvedev, V.Yu. Osipov, A.E. Alexenskii, A.Ya. Vul', Appl. Magn. Reson. 36 (2009) 317–329.
[16] L.B. Casabianca, A.I. Shames, A.M. Panich, O. Shenderova, L. Frydman, J. Phys. Chem. C 115 (2011) 19041–19048.
[17] T.M. Alam, Mater. Chem. Phys. 85 (2004) 310–315.
[18] A.M. Panich, A. Altman, A.I. Shames, V.Yu. Osipov, A.E. Alexenskiy, A.Ya. Vul', J. Phys. D Appl. Phys. 44 (2011) 125303/1-5.